Zhang et al. Nanoscale Research Letters (2017) 12:84
DOI 10.1186/s11671-017-1872-8

Nanoscale Research Letters

NANO EXPRESS Open Access

Effects of precursor solution composition on the performance and I-V hysteresis of perovskite solar cells based on $CH_3NH_3PbI_{3-x}Cl_x$

Z. L. Zhang[1], B. Q. Men[2], Y. F. Liu[1], H. P. Gao[1] and Y. L. Mao[1,3*]

Abstract

Precursor solution of $CH_3NH_3PbI_{3-x}Cl_x$ for perovskite solar cells was conventionally prepared by mixing $PbCl_2$ and CH_3NH_3I with a mole ratio of 1:3 ($PbCl_2$:CH_3NH_3I). While in the present study, $CH_3NH_3PbI_{3-x}Cl_x$-based solar cells were fabricated using the precursor solutions containing $PbCl_2$ and CH_3NH_3I with the mole ratios of 1:3, 1.05:3, 1.1:3, and 1.15:3, respectively. The results display that the solar cells with the mole ratio of 1.1:3 present higher power conversion efficiency and less I-V hysteresis than those with the mole ratio of 1:3. Based on some investigations, it is concluded that the higher efficiency could be due to the smooth and pinhole free film formation, high optical absorption, suitable energy band gap, and the large electron transfer efficiency, and the less I-V hysteresis may be attributed to the small low frequency capacitance of the device.

Keywords: I-V hysteresis, Precursor solution composition, $CH_3NH_3PbI_{3-x}Cl_x$

Background

Organometal halide perovskite solar cells (PSCs) have attracted much attention over the last several years due to their outstanding properties, such as large absorption coefficient, high electron-hole diffusion length, and high charge carrier mobility [1–6]. The power conversion efficiency (PCE) has increased from 3.8 to 22% [7]. The typical architectures of PSCs mainly contain electron transporting layer (ETL)/perovskite/hole transporting layer (HTL) (n-i-p) and HTL/perovskite/ETL (p-i-n) structures [8]. In the $CH_3NH_3PbX_3$ (X = I, Br, Cl) family, a mixed halide perovskite $CH_3NH_3PbI_{3-x}Cl_x$ ($MAPbI_{3-x}Cl_x$) has been proved a large diffusion length (~1 μm), which could be applied for planar heterojunction solar cells with improved device performance [9, 10]. Some groups have reported the results of the $MAPbI_{3-x}Cl_x$-based solar cells [11–13], in which the highest PCE is 19.3% [14].

The precursor solution of $MAPbI_{3-x}Cl_x$ is conventionally prepared by mixing $PbCl_2$ and CH_3NH_3I with a mole ratio of 1:3 ($PbCl_2$:CH_3NH_3I). While there was no or only trace amount of Cl to be detected [15, 16]. Some studies have been performed to investigate the role of Cl in the $MAPbI_{3-x}Cl_x$ film formation [17, 18]. A widely accepted opinion is that Cl ion in organometal halide perovskite can boost the mobility of excitons and the charge carrier transport [19–21]. A few groups have fabricated $MAPbI_{3-x}Cl_x$ solar cells using the precursor solutions containing excess $PbCl_2$ to investigate its effect on the performance of solar cells based on the I-V measurement with single scan direction [18, 21–23]. It has been reported that hysteretic effects were observed during the I-V measurement of the perovskite solar cells [24]. I-V hysteresis could lead to an over- or underestimation of the PCE if it is not considered. Up to now, there are few reports to investigate the effects of excess $PbCl_2$ on the PCE and I-V hysteresis of $MAPbI_{3-x}Cl_x$ solar cells by considering the hysteretic effect.

Therefore in the present study, $MAPbI_{3-x}Cl_x$-based solar cells were fabricated using the precursor solutions containing different mole ratios of $PbCl_2$, and CH_3NH_3I.

* Correspondence: ylmao1@163.com
[1]School of Physics and Electronics, Henan University, Kaifeng 475004, China
[3]Institute for Computational Materials Science, Henan University, Kaifeng 475004, China
Full list of author information is available at the end of the article

I-V measurements were carried out with reverse scan (RS) and forward scan (FS). The photovoltaic parameters were obtained from the I-V curves averaged with RS and FS. Based on the measurements, the effects of excess $PbCl_2$ on the PCE and the I-V hysteresis of the solar cells were investigated. One of the novelties of this work is that the photovoltaic parameters were obtained by an average of RS and FS to improve the accuracy of data. The other is the observation and investigation of the effect of excess $PbCl_2$ on I-V hysteresis.

Methods

Materials preparation

Methylammonium iodide (CH_3NH_3I) was synthesized with a method reported in the literature [25]. The perovskite precursor solutions (40 wt%) were obtained by mixing $PbCl_2$ and CH_3NH_3I (MAI) in anhydrous *N*,*N*-Dimethylformamide (DMF) at 60 °C with the mole ratios of 1:3, 1.05:3, 1.1:3, and 1.15:3 ($PbCl_2$ to MAI), respectively.

Solar cell fabrication

Perovskite solar cells with a structure of n-i-p were fabricated. FTO-coated glass substrate (~15 ohm/sq, NPG, Japan) was patterned and cleaned with detergent, acetone, 2-propanol, and ethanol for 15 min by sonication. Then the substrate was treated by oxygen plasma for 20 min. A hole-blocking layer of compact TiO_2 was deposited by spin-coating, a mildly acidic solution of titanium isopropoxide (Aladdin reagent) in ethanol (350 μl in 5 ml ethanol with 0.013 M HCl) at 2000 rpm for 30 s and annealed at 500 °C for 30 min. A mesoporous TiO_2 layer composed of commercial TiO_2 paste (Dyesol 18NRT, Dyesol) diluted in ethanol (1:3.5, weight ratio) was then deposited on the top of compact layer by spin-coating at 5000 rpm for 30 s. After drying at 125 °C, the TiO_2 films were annealed at 500 °C for 30 min. The perovskite precursor solution was spin-coated on the mesoporous TiO_2 film at 2000 rpm for 45 s in an argon-filled glove box. The sample was dried on a hotplate for 60 min at 110 °C. The hole-transporter layer was formed by spincoating a spiro-OMeTAD solution at 2000 rpm for 45 s. Finally, a gold layer with the thickness of 80 nm was deposited on top of the device by thermal evaporation in air.

Characterization

X-ray diffraction (XRD) patterns were carried out on a DX-2700 diffractometer. UV-vis absorption spectra were performed on a UV–vis spectrophotometer (Varian Cary 5000). Morphologies and microstructures were obtained by a scanning electron microscope (SEM, JEM-7001 F, JEOL). Photocurrent-voltage (I-V) curves were carried out with a Keithley 2440 Sourcemeter under AM 1.5 G illumination with 100-mW/cm^2 intensity from a Newport Oriel Solar Simulator. The active area of the device was 0.1 cm^2 determined with a mask. Steady-state photoluminescence (PL) and time-resolved photoluminescence (TRPL) spectra were collected using a fluorometer (FLS 980E, Edinburgh Photonics). Capacitance-frequency measurements were performed under a forward bias of

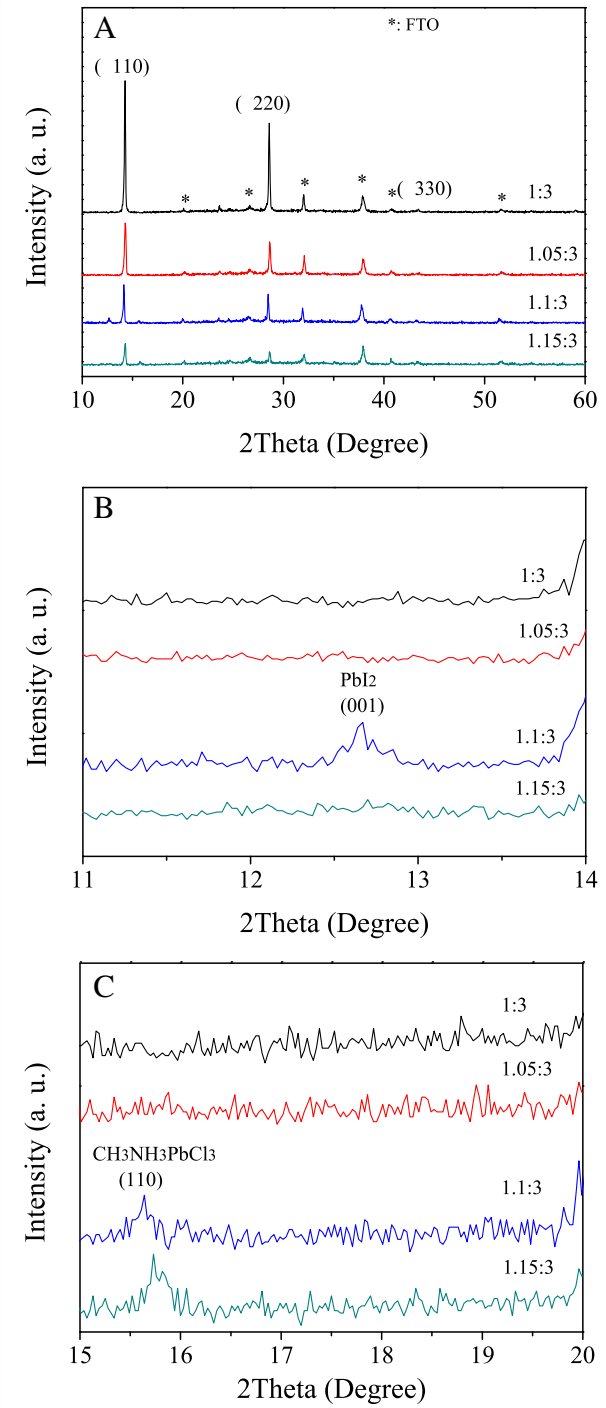

Fig. 1 XRD patterns of $MAPbI_{3-x}Cl_x$ films with different mole ratios at the range of (**a**) 10-60 degree, (**b**) 11-14 degree, and (**c**) 15-20 degree

0.6 V under 1 sun illumination conditions using an electrochemical workstation (RST5200, Zhengzhou Shiruisi Instrument Co., Ltd.) with the frequency range from 0.1 to 1000 Hz. The electrochemical impedance (IS) measurements were carried out with an electrochemical workstation (CHI660e, Shanghai CHI Co., Ltd.) in the frequency range from 0.1 to 100 kHz, in which an alternative signal with 5 mV magnitude was applied.

Results and discussion

Figure 1 shows the XRD patterns of $MAPbI_{3-x}Cl_x$ films with different mole ratios. Three main diffraction peaks at about 14.2°, 28.6°, and 43.1° are ascribed to (110), (220), and (330) lattice planes of halide perovskite with a tetragonal structure [26]. This indicates that the perovskite films with tetragonal structure are formed. A weak peak located at 12.7° for the sample with the ratio of 1.1:3 (Fig. 1b) can be assigned to the (001) diffraction peak of PbI_2 [10]. The peak at about 15.6° for the samples with the mole ratios of 1.1:3 and 1.15:3 (Fig. 1c) can be assigned to the (110) diffraction peak of $CH_3NH_3PbCl_3$ [18]. This agrees with the previous reports that Cl incorporation in an iodide-based structure was only at low concentration, and phase separation readily occurred with increased concentration [22, 27]. The PbI_2 phase appeared for the sample with the mole ratio of 1.1:3 and then disappeared for that with the mole ratio of 1.15:3 (Fig. 1b). While the $CH_3NH_3PbCl_3$ phase appeared in both the samples with the mole ratios of 1.1:3 and 1.15:3 (Fig. 1c). This is in accord with the reported $MAPbI_{3-x}Cl_x$ film growth process [23]. As a nucleation center, $PbCl_2$ induces the nucleation of PbI_2. PbI_2 acts with MAI to form the perovskite film and exhausts the available Pb ions to form $CH_3NH_3PbCl_3$.

Figure 2a shows the UV-vis absorption spectra of $MAPbI_{3-x}Cl_x$ films with different mole ratios. The absorption intensity increases firstly, and then decreases with the increase of mole ratio, which is the strongest at the mole ratio of 1.1:3. Figure 2b shows the absorption spectra of $MAPbI_{3-x}Cl_x$ films at the range from 730 to 800 nm. The absorption edge is obtained by extrapolating from the absorption of direct transition [28]. The band gap of $MAPbI_{3-x}Cl_x$ can be estimated from the absorption edge to be 1.573, 1.580, 1.598, and 1.596 eV for $MAPbI_{3-x}Cl_x$ with the mole ratio of 1:3, 1.05:3, 1.1:3, and 1.15:3, respectively.

Figure 3 shows the SEM images of the $MAPbI_{3-x}Cl_x$ films with different mole ratios. It is observed that some needle-like crystals for the film with the mole ratio of 1:3 (Fig. 3a). The films with the mole ratios of 1.05:3 and 1.15:3 become smooth and cover all the substrate with some small pinholes (Fig. 3b, d). At the mole ratio of 1.1:3, the pinholes disappeared and the substrate was fully covered by the $MAPbI_{3-x}Cl_x$ film (Fig. 3c). According to the previous reports [23, 29], $PbCl_2$ colloids in the precursor solution act as heterogeneous nucleation sites for the perovskite film formation. When excess $PbCl_2$ was introduced, the heterogeneous nucleation sites increased rationally, which possibly enhanced the morphology eventually. As the amount of $PbCl_2$ further increased, the grain size of the perovskite film slightly increased, and the surface becomes mother.

Figure 4a shows the PL spectra of $MAPbI_{3-x}Cl_x$ films with different mole ratios on FTO substrate. The peak at ~780 nm could be from the emission of $MAPbI_{3-x}Cl_x$ [9]. The PL intensities of the films with the mole ratios of 1.05:3, 1.1:3, and 1.15:3 are higher than that of 1:3. The TRPL spectra of $MAPbI_{3-x}Cl_x$ films with different mole ratios on FTO substrate are shown in Fig. 4b. The TRPL curve was fitted with an exponential diffusion model, and the exciton lifetime is 58, 79, 67, and 177 ns for the perovskite film with the mole ratio of 1:3, 1.05:3, 1.1:3, and 1.15:3, respectively. The exciton lifetimes of the films with the mole ratio of 1.05:3, 1.1:3, and 1.15:3 are longer than that of that of 1:3. The higher PL intensities could be due to their longer exciton lifetimes [30, 31]. The enhanced exciton lifetime indicates the reduced recombination in the $MAPbI_{3-x}Cl_x$ films. To investigate the charge transfer between $MAPbI_{3-x}Cl_x$ film and TiO_2, the PL spectra of $FTO/TiO_2/MAPbI_{3-x}Cl_x$ samples were performed and shown in Fig. 4c. Compared with the PL spectra of $FTO/MAPbI_{3-x}Cl_x$ (Fig. 4a), there is a quenching effect when the $MAPbI_{3-x}Cl_x$ layer contacts

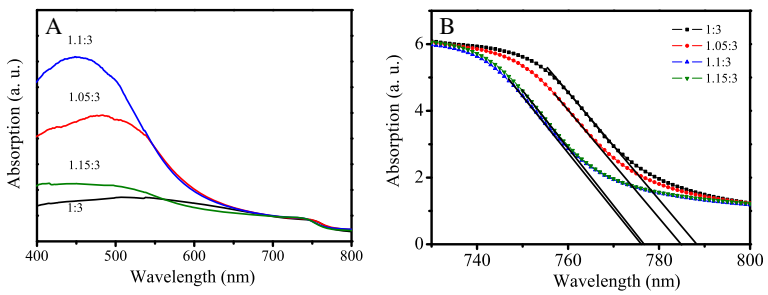

Fig. 2 UV-vis absorption spectra of $MAPbI_{3-x}Cl_x$ films with different mole ratios at the range of (**a**) 400-800 nm, and (**b**) 730-800 nm

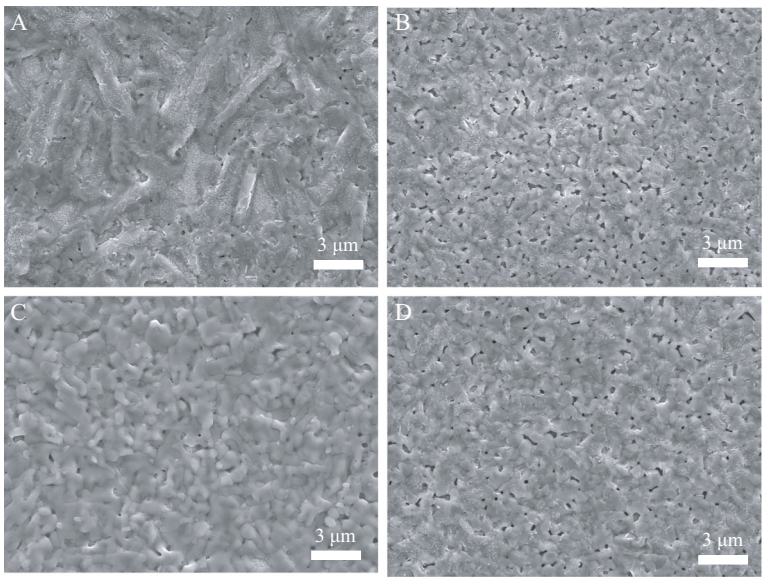

Fig. 3 SEM images of the $MAPbI_{3-x}Cl_x$ films with the mole ratio of (**a**) 1:3, (**b**) 1.05:3, (**c**) 1.1:3, and (**d**) 1.15:3

with TiO_2 film, which is due to the electron injection from $MAPbI_{3-x}Cl_x$ to TiO_2. The charge transfer efficiency can be estimated by the PL intensity ratio of FTO/TiO_2/$MAPbI_{3-x}Cl_x$ to FTO/$MAPbI_{3-x}Cl_x$, which is 0.25, 0.21, 0.19, and 0.24 for the perovskite films with the mole ratio of 1:3, 1.05:3, 1.1:3, and 1.15:3, respectively. The PL intensity ratio of the sample with the mole ratio of 1.1:3 is smaller than the others, which indicates a more efficient electron transfer to TiO_2. This could be due to a stronger interfacial coupling at the interface [32].

Perovskite solar cells were fabricated using the precursor solutions with different mole ratios with a structure of FTO/c-TiO_2/mp-TiO_2/$MAPbI_{3-x}Cl_x$/spiro-oMeTAD/Au. Figure 5 shows the photovoltaic parameters of the solar

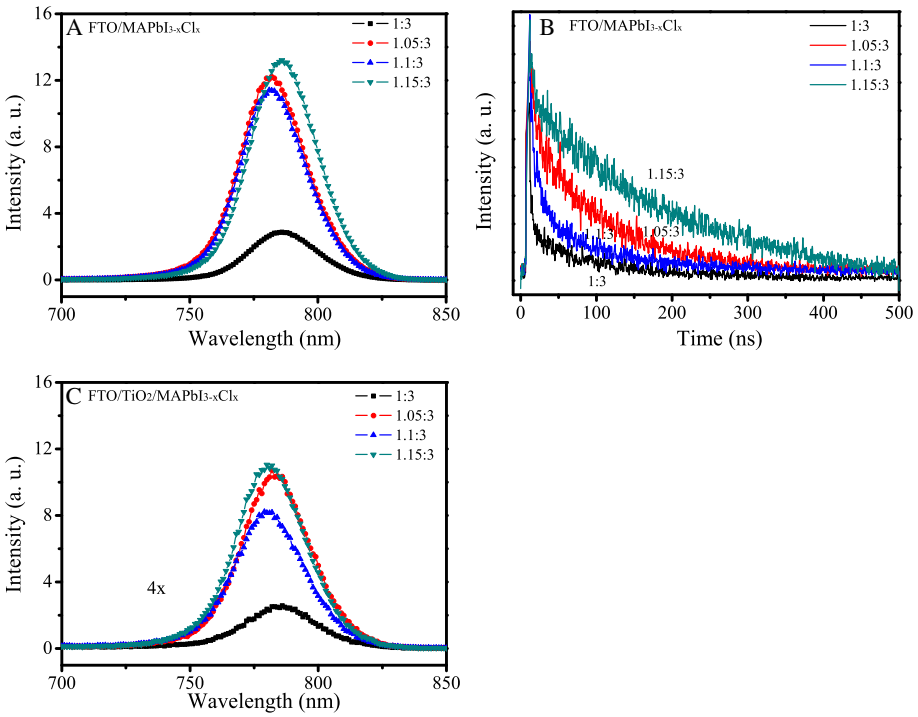

Fig. 4 a PL and **b** TRPL spectra of FTO/$MAPbI_{3-x}Cl_x$ samples. **c** PL spectra of FTO/TiO_2/$MAPbI_{3-x}Cl_x$ samples

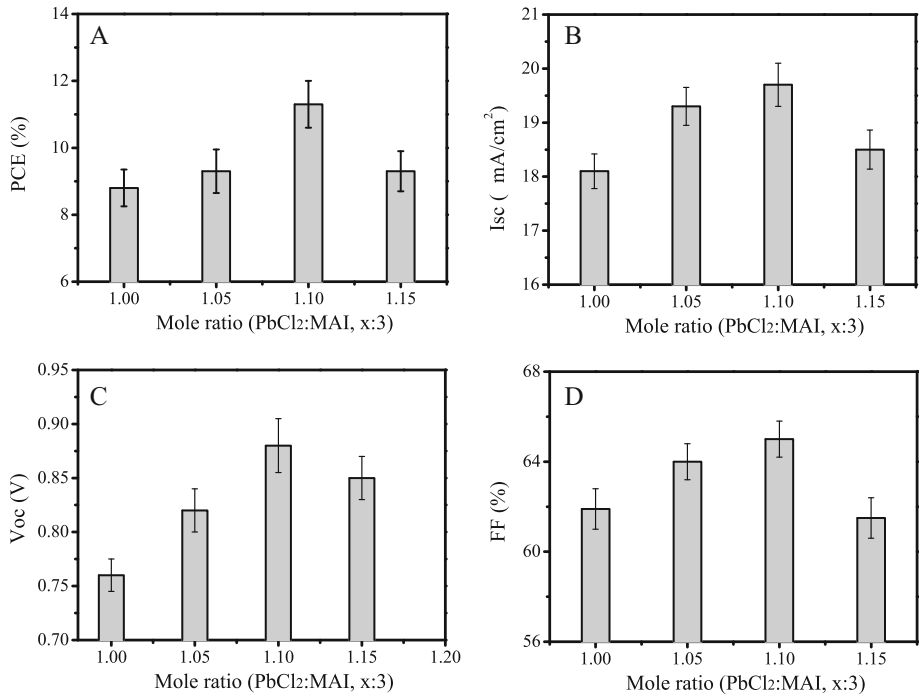

Fig. 5 Photovoltaic parameters of the solar cells using the precursor solutions with different mole ratios. **a** Isc, **b** Voc, **c** FF, and **d** PCE. The data were obtained from 20 pieces of devices for each of precursor solutions

cells, which were obtained from 20 pieces of devices for each of precursor solutions. The short current (J_{sc}), open voltage (V_{oc}), fill factor (FF) and power conversion efficiency (PCE) were obtained from I-V curves averaged with reverse scan (RS) and forward scan (FS). These parameters are listed in Table 1. With the increase of mole ratio, the parameters of the solar cells were firstly increased, and then decreased. The solar cells with the mole ratio of 1.1:3 present an enhanced performance. Compared with those of solar cells with the mole ratio of 1:3, the V_{oc}, J_{sc}, FF, and PCE of the solar cells with the mole ratio of 1.1:3 were increased to 0.88 V, 19.7 mA/cm^2, 65%, and 11.3% from 0.76 V, 18.1 mA/cm^2, 61.9%, and 8.8%, respectively.

Figure 6 shows the current density-voltage (I-V) curves of the best solar cells using the precursor solutions with different mole ratios. It was found that the degree of I-V hysteresis depends on the precursor composition. This phenomenon was always observed in our experiments. I-V hysteresis index (HI) is defined by the following equation [33],

$$\text{hysteresis index} = \frac{J_{RS}(0.8V_{oc}) - J_{FS}(0.8V_{oc})}{J_{RS}(0.8V_{oc})}$$

where $J_{RS}(0.8V_{oc})$ and $J_{FS}(0.8V_{oc})$ stand for the photocurrent density at 80% of V_{oc} for the RS and FS, respectively. The calculated hysteresis index values are 0.164, 0.085, 0.019, and 0.066 for the I-V curves with the mole ratio of 1:3, 1.05:3, 1.1:3, and 1.15:3, respectively. With the increase of mole ratio, the hysteresis degree first decreases, and then increases. At the mole ratio of 1.1:3, the hysteresis index value is the smallest. The high PCE of 11.55% with less I-V hysteresis was obtained using the precursor solution with the mole ratio of 1.1:3.

Table 1 Photovoltaic parameters of perovskite solar cells as a function of different mole ratios of $PbCl_2$ and MAI

$PbCl_2$:MAI	V_{oc} (V)	J_{sc} (mA/cm^2)	FF (%)	η (%)
1:3	0.76 ± 0.01	18.1 ± 0.2	61.9 ± 1.6	8.8 ± 0.1
1.05:3	0.82 ± 0.02	19.3 ± 0.3	64.0 ± 1.5	9.3 ± 0.2
1.1:3	0.88 ± 0.01	19.7 ± 0.1	65.0 ± 0.5	11.3 ± 0.2
1.15:3	0.85 ± 0.01	18.5 ± 0.2	61.5 ± 1.5	9.3 ± 0.3

To get an insight into the enhanced performance and less I-V hysteresis of the solar cells with the mole ratio of 1.1:3, some investigations were performed. Based on the energy band gaps calculated from the absorption spectra (Fig. 2) and the literature [33], the energy band diagrams of TiO_2, $MAPbI_{3-x}Cl_x$, and Spiro-OMeTAD are shown in Fig. 7. The conduction band offset between $MAPbI_{3-x}Cl_x$ and TiO_2 is the largest for the mole ratio of 1.1:3 due to its wide band gap, which might be one of the reasons to present a higher voltage [28]. Moreover, the larger conduction band offset might contribute to its increased current density, because the band offset has

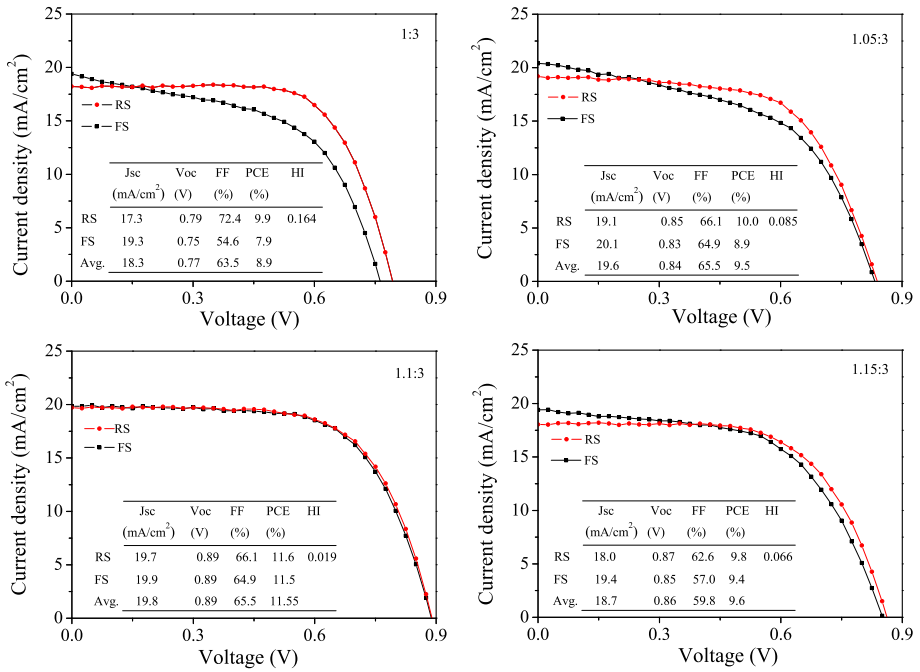

Fig. 6 Current density-voltage (I-V) curves of the best solar cells using the precursor solutions with different mole ratios

been proved to be a driving force for charge transfer between conduction bands in the heterojunction [34, 35]. This speculation was confirmed by the photoluminescence (PL) results.

Hysteretic effects during I-V measurements have been observed in perovskite solar cells. It has been proposed that the slow decay process of the capacitive charging or discharging current during voltage sweep induces the non-steady state photocurrent and I-V hysteresis [33, 36, 37]. The non-steady state photocurrents could be due to the capacitance at low frequency (0.1 ~ 1 Hz) resulting from electrode polarization at perovskite/electrode interfaces [33]. To understand the I-V hysteresis of the solar cells with different precursor compositions, the capacitance of the devices were directly measured with an electrochemical workstation. Figure 8 shows the dependence of capacitance on frequency. The low frequency capacitance (C_{LF}) is observed near 10^{-1} Hz. With the increase of the mole ratio, C_{LF} decreases firstly, and then increases, which is the smallest at the mole ratio of 1.1:3. The smaller C_{LF} indicates the less polarization which could be the origin of the I-V hysteresis [33]. The variation of C_{LF} with the mole ratio agrees with the I-V hysteresis tendency shown in Fig. 4.

To investigate the reason of capacitance decrease, the impedance spectra of the solar cells were measured. Figure 9a shows the Nyquist plots of the cells based on

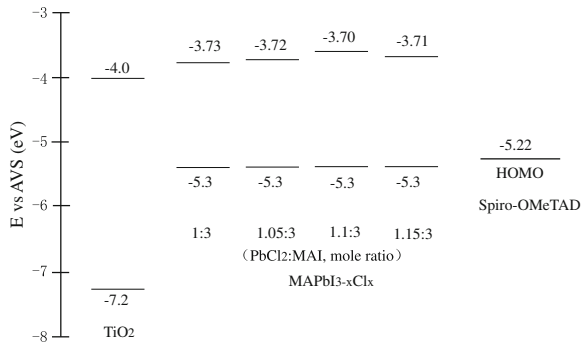

Fig. 7 Schematic of the energy band diagrams of TiO_2, $MAPbI_{3-x}Cl_x$, and Spiro-OMeTAD.

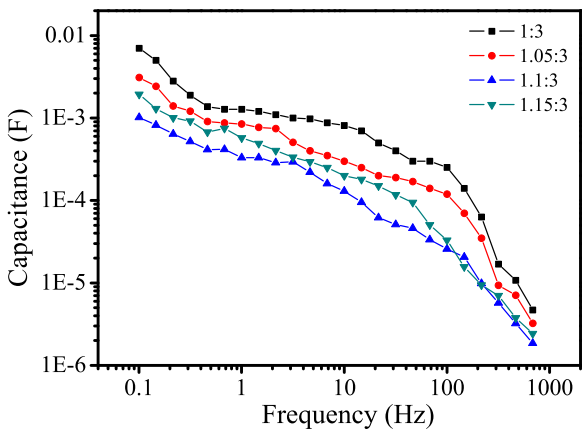

Fig. 8 Capacitance-frequency plots of the solar cells directly measured from an electrochemical workstation

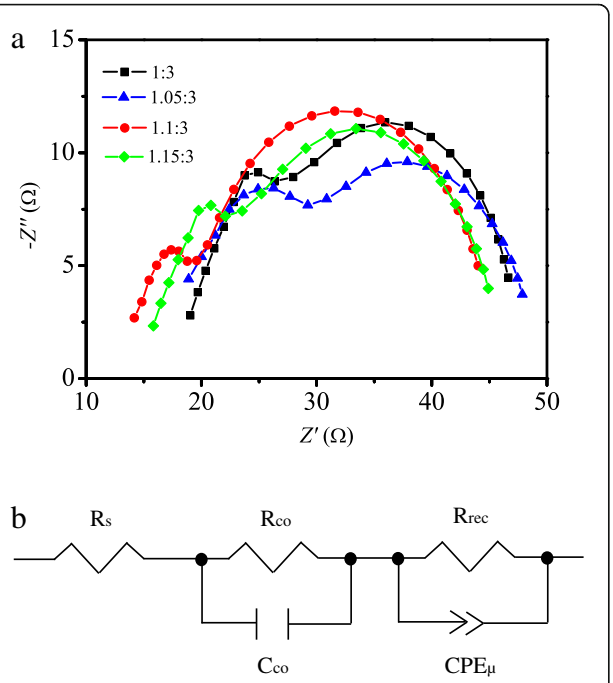

Fig. 9 a Typical Nyquist plots for the perovskite solar cells. The simulation result (*solid line*) is fitted to experimental data (*symbols*). **b** Equivalent circuit applied to fit the Nyquist plots

the different mole ratios, in which the symbols are the experimental data and the solid lines are the fitting results. There are two RC arcs contained in the plots. Figure 9b shows the equivalent circuit used to fit the data. The high-frequency RC element could be ascribed to the contact resistance (R_{co}) at the interfaces, while the low-frequency element may be attributed to the recombination resistance (R_{rec}) and chemical capacitance (C_{μ}) of the device, and the R_s is a series resistance [38]. The parameters obtained by fitting are listed in Table 2. The R_{co} (10.6 Ω) of solar cells based on precursor solution with mole ratio of 1.1:3 is smaller than that of the other precursor solution. This indicates that the perovskite film with the mole ratio of 1.1:3 provides better contact with electron transporting layer and hole transporting layer than the other perovskite film. Thus, the decreased capacitance of the solar cells with the mole ratio of 1.1:3 could be due to the better contact of perovskite film with ETL and HTL [39].

Table 2 Fitting parameters for EIS data

Sample	R_s/Ω	R_{co}/Ω	R_{rec}/Ω	C_{co}/F	CPE-T/F
1:3	17.7	21.0	23.7	1.5E-7	3.6E-6
1.05:3	17.1	17.8	27.5	1.6E-8	2.5E-6
1.1:3	13.5	10.6	28.5	1.2E-7	6.9E-7
1.15:3	15.2	16.8	27.6	1.3E-7	5.1E-6

Conclusion

The solar cells based on $MAPbI_{3-x}Cl_x$ were fabricated using the precursor solutions containing the mole ratio of 1:3, 1.05:3, 1.1:3, and 1.15:3. I-V curves were obtained by both reverse scan and forward scan, from which the photovoltaic parameters were calculated by taking the average of them. The results displayed that the solar cells with the mole ratio of 1.1:3 present higher PCE and less I-V hysteresis. To get an insight into the results, some investigations were performed. The higher PCE could be due to the smooth and pinhole-free film formation, high optical absorption, suitable energy band gap, and the large electron transfer efficiency. The less I-V hysteresis may be attributed to the small low frequency capacitance of the device.

Funding

This work is supported by the NSFC-Henan Province Joint Fund (U1604144), Science Fund of Henan Province (162300410020), National Science Research Project of Education Department of Henan Province (No.17A140005), Science and Technology Development Project of Henan Province (No.142102210389), and Program for Innovative Research Team (in Science and Technology) in University of Henan Province (No. 13IRTSTHN017).

Authors' contributions

Z-LZ, B-QM, and Y-LM carried out the main part of experiment and drafted the manuscript. Other authors provided assistance with experimental measurements, data analysis, and the manuscript writing. All authors read and approved the final manuscript.

Competing interests

The authors declare that they have no competing interests.

Author details

[1]School of Physics and Electronics, Henan University, Kaifeng 475004, China. [2]Henan Vocational College of Agriculture, Zhongmu 451450, China. [3]Institute for Computational Materials Science, Henan University, Kaifeng 475004, China.

Received: 17 December 2016 Accepted: 28 January 2017
Published online: 03 February 2017

References

1. Dong Q, Fang Y, Shao Y, Mulligan P, Qiu J, Cao L, Huang J (2015) Electron-hole diffusion lengths > 175 μm in solution-grown $CH_3NH_3PbI_3$ single crystals. Science 347:967–970
2. Chen LC, Chen JC, Chen CC, Wu CG (2015) Fabrication and properties of high-efficiency perovskite/PCBM organic solar cells. Nanoscale Res Lett 10:312
3. Zhu L, Shi J, Lv S, Yang S, Xu X, Xu Y, Xiao J, Wu H, Luo Y, Li D, Meng Q (2015) Temperature-assisted controlling morphology and charge transport property for highly efficient perovskite solar cells. Nano Energy 15:540–548
4. Jeon NJ, Noh JH, Yang WS, Kim YC, Ryu SC, Seo JW, Seok SI (2015) Compositional engineering of perovskite materials for high-performance solar cells. Nature 517:476–480
5. Liu DT, Li SB, Zhang P, Wang YF, Zhang R, Sarvarib H, Wang F, Jiang Wu J, Wang ZM, Chen ZD (2017) Efficient planar heterojunction perovskite solar cells with Li-doped compact TiO_2 layer. Nano Energy 31:462–468
6. Li SB, Zhang B, Wang YF, Sarvari H, Liu DT, Wu J, Yang YJ, Wang ZM, Zhi David Chen ZD (2016) Interface engineering of high efficiency perovskite solar cells based on ZnO nanorods using atomic layer deposition. Nano Res. doi:10.1007/s12274-016-1407-0
7. National renewable energy laboratory best research-cell efficiencies. www.nrel.gov/ncpv/images/efficiency_chart.jpg . Accessed 17 May 2016.
8. Habibi M, Zabihi F, Ahmadian-Yazdi MR, Eslamian M (2016) Progress in emerging solution-processed thin film solar cells-Part II:Perovskite solar cells. Renew Sust Energ Rev 62:1012–1031

9. Stranks SD, Eperon GE, Grancini G, Menelaou C, Alcocer MJP, Leijtens T, Laura M, Herz M, Petrozza A, Snaith HJ (2013) Electron-hole diffusion lengths exceeding 1 micrometer in an organometal trihalide perovskite absorber. Science 342:341–344
10. Edri E, Kirmayer S, Henning A, Mukhopadhyay S, Gartsman K, Rosenwakes Y, Hodes G, Cahen D (2014) Why lead methylammonium tri-iodide perovskite-based solar cells require a mesoporous electron transporting scaffold. Nano Lett 14:1000–1004
11. Wang W, Zhang ZB, Cai YY, Chen JS, Wang JM, Huang RY, Lu XB, Gao XS, Shui LL, Wu SJ, Liu JM (2016) Enhanced performance of $CH_3NH_3PbI_{3-x}Cl_x$ perovskite solar cells by CH_3NH_3I modification of TiO_2-perovskite layer interface. Nanoscale Res Lett 11:316
12. Liang PW, Liao CY, Chueh CC, Zuo F, Williams ST, Xin XK, Lin J, Jen AK (2014) Additive enhanced crystallization of solution processed perovskite for highly efficient planar-heterojunction solar cells. Adv Mater 26:3748–3754
13. Ahmadian-Yazdi MR, Zabihi F, Habibi M, Eslamian M (2016) Effects of process parameters on the characteristics of mixed-halide perovskite solar cells fabricated by one-step and two-step sequential coating. Nanoscale Res Lett 11:408–418
14. Zhou HP, Chen Q, Li G, Luo S, Song T, Duan H, Hong Z, You J, Liu Y, Yang Y (2014) Interface engineering of highly efficient perovskite solar cells. Science 345:542–546
15. Chen Q, Zhou HP, Fang YH, Stieg AZ, Song TB, Wang HH, Xu XB, Liu YS, Lu SR, You JB, Sun P, Mckay J, Goorsky MS, Yang Y (2015) The optoelectronic role of chlorine in $CH_3NH_3PbI_3$(Cl)-based perovskite solar cells. Nat Commun 6:7269–7277
16. Colella S, Mosconi E, Pellegrino G, Alberti A, Guerra VLP, Masi SA, Listoi A, Rizzo A, Condorelli GG, Angelis FD, Gigli G (2014) Elusive presence of chloride in mixed halide perovskite solar cells. J Phys Chem Lett 5:3532–3538
17. Williams ST, Zuo F, Chueh CC, Liao CY, Liang PW, Jen AKY (2014) Role of chloride in the morphological evolution of organo-lead halide perovskite thin films. ACS Nano 8:10640–10654
18. Yu H, Wang F, Xie FY, Li WW, Chen J, Zhao N (2010) The role of chlorine in the formation process of $CH_3NH_3PbI_{3-x}Cl_x$ Perovskite. Adv Funct Mater 24:7102–7108
19. Zabihi F, Ahmadian-Yazdi MR, Eslamian M (2016) Fundamental study on the fabrication of inverted planar perovskite solar cells using two-step sequential substrate vibration-assisted spray coating (2S-SVASC). Nanoscale Res Lett 11:71
20. Zhang M, Yu H, Lyu MQ, Wang Q, Yun JH, Wang LZ (2014) Composition-dependent photoluminescence intensity and prolonged recombination lifetime of perovskite $CH_3NH_3PbBr_{3-x}Cl_x$ films. Chem Commun 50:11727
21. Colella S, Mosconi E, Fedeli P, Listorti A, Gazza F, Orlandi F, Ferro P, Besagni T, Rizzo A, Calestani G, Gigli G, Angelis DF, Mosca R (2013) MAPbI3-xClx mixed halide perovskite for hybrid solar cells: The role of chloride as dopant on the transport and structural properties. Chem Mater 25:4613
22. Mcleod JA, Wu ZW, Sun BQ, Liu LJ (2016) The influence of the I/Cl ratio on the performance of $CH_3NH_3PbI_{3-x}Cl_x$-based solar cells: why is CH_3NH_3I:$PbCl_2$ = 3:1 the "magic" ratio. Nanoscale 8:6361–6368
23. Huang C, Fu NQ, Liu FY, Jiang LX, Hao XJ, Huang HT (2016) Highly efficient perovskite solar cells with precursor composition-dependent morphology. Sol Energy Mater Sol Cells 145:231–237
24. Unger EL, Hoke ET, Bailie CD, Nguyen WH, Bowring AR, Heumuller T, Christoforod MG, McGehee MD (2014) Hysteresis and transient behavior in current-voltage measurements of hybrid-perovskite absorber solar cells. Energy Environ Sci 7:3690–3698
25. Lee MM, Teuscher J, Miyasaka T, Murakami TN, Snaith HJ (2012) Efficient hybrid solar cells based on meso-superstructured organometal halide perovskites. Science 338:643–647
26. Stoumpos CC, Malliakas CD, Kanatzidis MG (2013) Semiconducting tin and lead iodide perovskites with organic vations: phase transitions, high mobilities, and near-infrared photoluminescent properties. Inorg Chem 52:9019–9038
27. Yin WJ, Shi T, Yan Y (2014) Unique properties of halide perovskites as possible origins of the superior solar cell performance. Adv Mater 26:4653–4658
28. Li YL, Sun WH, Yan WB, Ye SY, Peng HT, Liu ZW, Bian ZQ, Huang CH (2015) High-performance planar solar cells based on $CH_3NH_3PbI_{3-x}Cl_x$ perovskites with determined chlorine mole fraction. Adv Funct Mater 25:4867–4873
29. Tidhar Y, Edri E, Weissman H, Zohar D, Hodes G, Cahen D, Rybtchinski B, Kirmayer S (2014) Crystallization of methylammonium lead halide perovskites: implications for photovoltaic applications. J Am Chem Soc 136:13249–13256
30. Chen LC, Chen CC, Chen JC, Wu CG (2015) Annealing effects on high-performance $CH_3NH_3PbI_3$ perovskite solar cells prepared by solution-process. Sol Energy 122:1047–1051
31. Roldan C, Gratia P, Zimmermann I, Grancini G, Gao P, Graetzel M, Nazeeruddin MK (2015) High efficiency methylammonium lead triiodide perovskite solar cells: the relevance of non-stoichiometric precursors. Energy Environ Sci 8:3550–3556
32. Mosconi E, Ronca E, Angelis FD (2014) First-principles investigation of the TiO_2/organohalide perovskites interface: The role of interfacial chlorine. J Phys Chem Lett 5:2619–2625
33. Kim HS, Park NG (2014) Parameters affecting I-V hysteresis of $CH_3NH_3PbI_3$ perovskite solar cells: effects of perovskite crystal size and mesoporous TiO_2 layer. J Phys Chem Lett 5:2927-2934
34. Robel I, Kuno M, Kamat PV (2007) Size-dependent electron injection from excited CdSe quantum dots into TiO_2 nanoparticles. J Am Chem Soc 129:4136–4137
35. Tvrdy K, Frantszov P, Kamat PV (2011) Photoinduced electron transfer from semiconductor quantum dots to metal oxide nanoparticles. Proc Natl Acad Sci U S A 108:29–34
36. Sanchez RS, Gonzalez VP, Lee JW, Park NG, Kang YS, Mora SI, Bisquert J (2014) Slow dynamic processes in lead halide perovskite solar cells. J Phys Chem Lett 5:2357–2363
37. Kim HS, Mora SI, Gonzalez PV, Fabregat SF, Juarez-Perez EJ, Park NG, Bisquert J (2013) Mechanism of carrier accumulation in perovskite thin-absorber solar cells. Nat Commun 4:2242–2248
38. Kim HS, Lee JW, Yantara N, Boix PP, Kulkarni SA, Mhaisalkar S, Gratzel M, Park NG (2013) High efficiency solid-state sensitized solar cell-based on submicrometer rutile TiO_2 nanorod and $CH_3NH_3PbI_3$ perovskite sensitizer. Nano Lett 13:2412–2417
39. Kim HS, Jang IH, Ahn N, Choi M, Guerrero A, Bisquert J, Park NG (2015) Control of I-V hysteresis in $CH_3NH_3PbI_3$ perovskite solar cell. J Phys Chem Lett 6:4633–4639